

Porous Coordination Polymer Polymorphs with Different Flexible Pores Using a Structurally Flexible and Bent 1,3-Bis(4-pyridyl)propane Ligand

Katsuo Fukuhara,[†] Shin-ichiro Noro,^{*,†,‡,§} Kuniyoshi Sugimoto,^{||} Tomoyuki Akutagawa,[⊥] Kazuya Kubo,^{†,‡} and Takayoshi Nakamura^{*,†,‡}

[†]Graduate School of Environmental Science, Hokkaido University, Sapporo 060-0810, Japan

[‡]Research Institute for Electronic Science, Hokkaido University, Sapporo 001-0020, Japan

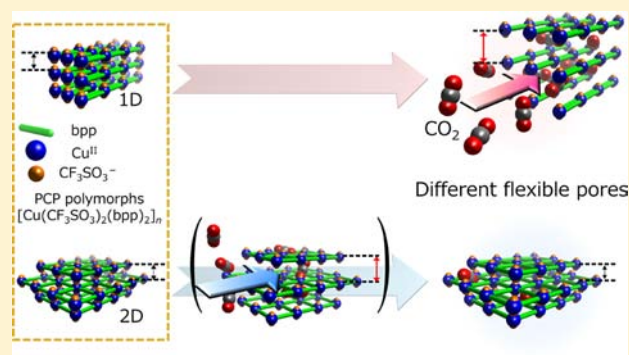
[§]PRESTO, Japan Science and Technology Agency (JST), 4-1-8 Honcho, Kawaguchi, Saitama 332-0012, Japan

^{||}Research & Utilization Division, Japan Synchrotron Radiation Research Institute, Hyogo 679-5198, Japan

[⊥]Institute for Multidisciplinary Research for Advanced Materials (IMRAM), Tohoku University, 1-1 Katahira, Aoba-ku, Sendai 980-8577, Japan

Supporting Information

ABSTRACT: Porous coordination polymer (PCP) polymorphs with the formula $[\text{Cu}(\text{CF}_3\text{SO}_3)_2(\text{bpp})_2]_n$ [**1** and **2**, where bpp = 1,3-bis(4-pyridyl)propane] have been synthesized and crystallographically characterized, and their distinguishable porous properties have been investigated. **1** was obtained by the removal of guest acetone molecules from one-dimensional PCP $\{[\text{Cu}(\text{CF}_3\text{SO}_3)_2(\text{bpp})_2] \cdot \text{CF}_3\text{SO}_3 \cdot 2\text{acetone}\}_n$ (**1**⊃acetone), while **2** was derived from two-dimensional PCP $\{[\text{Cu}(\text{CF}_3\text{SO}_3)_2(\text{bpp})_2] \cdot \text{H}_2\text{O}\}_n$ (**2**⊃H₂O) by the loss of guest H₂O molecules. The desolvated PCPs **1** and **2** with the same formula $[\text{Cu}(\text{CF}_3\text{SO}_3)_2(\text{bpp})_2]$ showed distinguishable structures, suggesting PCP polymorphs. In addition, their adsorption behaviors were completely different: **1** showed adsorption with the structural transformation from closed to open forms, while **2** appeared to expand its framework for only as long as was required for the passage of guest molecules. To the best of our knowledge, PCP polymorphs showing either of two different types of flexible pores are very rare.



INTRODUCTION

Porous coordination polymers (PCPs) and metal–organic frameworks (MOFs) consisting of metal ions, bridging ligands, and other units have attracted much attention because they afford diverse, regular, light, and flexible porous frameworks showing high performance and unprecedented storage, separation, and catalytic properties, by careful selection and combination of their building blocks.¹ In general, the structural diversity of PCP frameworks is easily realized by changing some of the components that build up the porous frameworks. On the other hand, PCP polymorphs with the same formula can have different porous frameworks, which could lead to increased structural diversification of PCPs. However, there are limited examples in which PCP systems using a polymorphism controlled not only crystal structures but also porous properties.^{2–5}

Two polymorphs of $[\text{Zn}_2(1,4\text{-bdc})_2(\text{dabco})]_n$ (1,4-bdc²⁻ = 1,4-benzenedicarboxylate; dabco = diazabicyclo[2.2.2]octane) have been reported: one was a tetragonal framework,^{2a} in which two-dimensional square-grid sheets constructed using Zn^{II}

paddle-wheel units and 1,4-bdc²⁻ were connected by dabco pillar ligands, while the other was a trigonal framework^{2b} with two-dimensional Kagomé nets as layers. Selective syntheses of these polymorphs were achieved by the templating effect of solvents in solvothermal reactions^{2b} and that of anions for mechanochemical synthesis^{2c} and simply by changing the crystallization temperature.^{2d} A three-dimensional PCP, $[\text{Zn}_2(\text{btdc})_2(4,4'\text{-bpy})]_n$ (btdc²⁻ = 2,2'-bithiophene-5,5'-dicarboxylate; 4,4'-bpy = 4,4'-bipyridine), also had two polymorphs: one was a 2-fold interpenetrated framework, and the other was a 3-fold one; they were obtained separately by employing different crystallization solvents. They showed different adsorption behavior and permanent and flexible porosities, which were attributed to the difference in the degree of interpenetration.³ In these systems, the polymorphism is mainly caused by the difference in connectivity between metal ions and bridging ligands or an aggregate state of PCP frameworks.

Received: September 6, 2012

Published: March 25, 2013

Table 1. Crystallographic Data for 1 Δ 2acetone, 2 Δ H₂O, and 3 Δ DMF·toluene

	1 Δ 2acetone	2 Δ H ₂ O	3 Δ DMF·toluene
formula	C ₃₄ H ₄₀ Cu ₁ F ₆ N ₄ O ₈ S ₂	C ₂₈ H ₃₀ Cu ₁ F ₆ N ₄ O ₇ S ₂	C ₃₈ H ₄₃ Cu ₁ F ₆ N ₅ O ₇ S ₂
fw	874.36	776.22	923.46
cryst syst	orthorhombic	monoclinic	monoclinic
a (Å)	12.3248(6)	9.0545(5)	13.3195(8)
b (Å)	17.1869(6)	17.7259(7)	23.2763(14)
c (Å)	19.2754(7)	10.9172(5)	13.8909(10)
α (deg)	90	90	90
β (deg)	90	96.9540(16)	102.4925(19)
γ (deg)	90	90	90
V (Å ³)	4083.0(3)	1739.30(14)	4204.6(5)
space group	Cmc2 ₁	P2 ₁	P2 ₁ /n
Z	4	2	4
D _c (g cm ⁻³)	1.422	1.482	1.459
F ₀₀₀	1804.00	794.00	1908.00
μ (Mo K α) (cm ⁻¹)	7.158	8.278	6.990
λ (Å)	0.71073	0.71073	0.71073
T (K)	173	173	173
R1 [$I > 2.00\sigma(I)$] ^a	0.0452	0.0293	0.0822
R (all reflns) ^a	0.0466	0.0316	0.1247
wR2 (all reflns) ^b	0.1278	0.0817	0.2466
GOF	1.050	1.047	1.062
no. of obsvns	4832	7745	7960
no. of variables	274	435	532

$$^a R1 = R = \sum |F_o| - |F_c| / \sum |F_o|. \quad ^b wR2 = [(\sum w(|F_o|^2 - |F_c|^2)^2) / \sum w(F_o^2)^2]^{1/2}.$$

Utilization of bridging ligands with structurally flexible parts is another very effective method for the construction of PCP polymorphs. For example, the 5,5'-methylenediisophthalate (mdip²⁻) ligand has two extreme conformations derived from the flexible methylene part: a form with C_s point group symmetry, in which the two benzene rings of mdip²⁻ are perpendicular to each other, and a C_{2v} form, which can be generated by symmetry with one-fourth of the ligand. Using this flexible ligand, two polymorphs of [Cu₂(mdip)]_n were formed: one has both C_s and C_{2v} forms, and the other possesses only the C_{2v} form. They had different three-dimensional permanent porous frameworks and different surface areas.⁴

In this contribution, we focus on the flexible and bent bridging ligand 1,3-bis(4-pyridyl)propane (bpp) to construct PCP polymorphs. The bpp ligand with a flexible trimethylene part can supply a variety of structural conformations (TT, TG, GG, and GG', where T = trans and G = gauche) that display quite different N–N distances and bend angles.⁶ In addition, the bent ligand enables the formation of one-, two-, and three-dimensional topologies with the same formula of [M(bpp)₂]_n.⁷ The conformation of the ligand and the topology in bpp-bridged PCP frameworks depends not only on the metal salts employed but also on the synthetic conditions such as solvents, temperature, and pH.⁸ Hence, PCP polymorphs based on bpp ligands could be obtained by finding the appropriate synthetic conditions for each polymorph.

Here, we report the synthesis and porous properties of PCP polymorphs of [Cu(CF₃SO₃)₂(bpp)₂]_n (**1** and **2**) obtained by simply changing the crystallization solvents. The two polymorphs showed not only considerably different framework topologies (one-dimensional doubly linked chain and a two-dimensional sheet) but also porous properties (different types of flexible pores). A one-dimensional coordination polymer of [Cu(CF₃SO₃)₂(bpp)₂(DMF)]·CF₃SO₃·toluene (**3 Δ** DMF·toluene, where DMF = *N,N*-dimethylformamide) was also

synthesized to clarify the coordination environments around the Cu^{II} centers in the PCP polymorphs.

EXPERIMENTAL SECTION

Materials. All reagents and chemicals were obtained from commercial sources.

Synthesis of [Cu(CF₃SO₃)₂(bpp)₂]·CF₃SO₃·2acetone]_n (1 Δ 2acetone). An acetone solution (10 mL) of Cu(CF₃SO₃)₂ (396 mg, 1.00 mmol) was slowly added to an acetone solution (10 mL) of bpp (362 mg, 2.00 mmol). The resulting purple microcrystals were filtered, washed with acetone, and dried in a vacuum at 373 K, forming the desolvated compound [Cu(CF₃SO₃)₂(bpp)₂]_n (**1**). Yield: 693 mg, 91%. Elem anal. Calcd for **1** (C₂₈H₂₈Cu₁F₆N₄O₆S₂): C, 44.35; H, 3.72; N, 7.39. Found: C, 44.17; H, 3.70; N, 7.34. Single crystals of 1 Δ 2acetone suitable for X-ray analysis were prepared by a diffusion method with a straight glass tube.

Synthesis of [Cu(CF₃SO₃)₂(bpp)₂]·H₂O]_n (2 Δ H₂O). An H₂O solution (10 mL) of Cu(CF₃SO₃)₂ (362 mg, 1.00 mmol) was slowly added to a MeOH solution (10 mL) of bpp (396 mg, 2.00 mmol). The resulting purple microcrystals were filtered, washed with H₂O and MeOH, and dried in a vacuum at 373 K, forming the desolvated compound [Cu(CF₃SO₃)₂(bpp)₂]_n (**2**). Yield: 603 mg, 80%. Elem anal. Calcd for **2** (C₂₈H₂₈Cu₁F₆N₄O₆S₂): C, 44.35; H, 3.72; N, 7.39. Found: C, 44.05; H, 3.71; N, 7.36. Single crystals of 2 Δ H₂O suitable for X-ray analysis were prepared by a diffusion method with a straight glass tube.

Synthesis of 3 Δ DMF·toluene. Single crystals suitable for X-ray analysis were prepared by the careful diffusion of toluene into a DMF solution of Cu(CF₃SO₃)₂ (54.2 mg, 0.150 mmol) and bpp (59.4 mg, 0.300 mmol) in a straight glass tube. After a few days, blue crystals were obtained. Yield: 114 mg, 93%. Elem anal. Calcd for 3 Δ DMF (C₃₁H₃₅Cu₁F₆N₅O₇S₂): C, 44.79; H, 4.24; N, 8.42. Found: C, 45.03; H, 4.66; N, 8.75.

Single-Crystal X-ray Diffraction (XRD). XRD measurements of 1 Δ 2acetone, 2 Δ H₂O, and 3 Δ DMF·toluene were performed using a Rigaku R-Axis-RAPID imaging plate diffractometer with graphite-monochromated Mo K α radiation ($\lambda = 0.71073$ Å). The data were corrected for Lorentz and polarization effects. The structures were

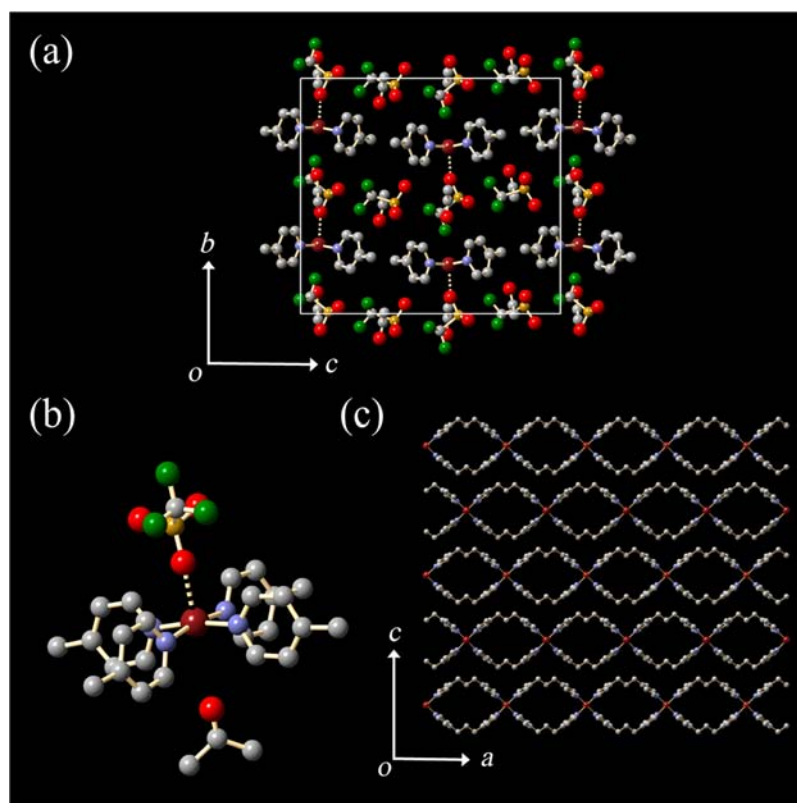


Figure 1. Crystal structure of 1D2acetone. (a) Unit cell viewed along the a axis. (b) Coordination environment around the Cu^{II} center. (c) One-dimensional doubly linked chain structure projected along the b axis (acetone and CF_3SO_3^- molecules are omitted for clarity). In all parts, the hydrogen atoms are omitted for clarity. Vermilion is for copper, blue for nitrogen, gray for carbon, red for oxygen, green for fluorine, and orange for sulfur.

solved using direct methods (*SHELXS-97*) and expanded using Fourier techniques.⁹ All non-hydrogen atoms were refined anisotropically. All hydrogen atoms were refined using the riding model. The refinements were carried out using full-matrix least-squares techniques on F^2 using *SHELXL-97*.⁹ The crystals of 1D2acetone and 2D H_2O were suggested by the program *SHELXL-97* to be a racemic twin with BASF twin factors 0.411(14) and 0.628(8), respectively. The Friedel pairs (2313 and 3665 for 1D2acetone and 2D H_2O , respectively) of reflections were not merged. The crystal data are summarized in Table 1. The crystallographic data in CIF format are available from the Cambridge Crystallographic Data Centre under CCDC reference numbers 912116 (1D2acetone), 912117 (2D H_2O), and 912118 (3D $\text{DMF}\cdot\text{toluene}$).

Physical Measurements. Elemental analyses (C, H, and N) were performed using a Yanaco CHN corder MT-6. The attenuated total reflection infrared (ATR-IR) spectra were recorded on a Thermo Nicolet iS10 FT-IR spectrometer equipped with a GladiATR accessory with a resolution of 4 cm^{-1} . Temperature-dependent microscopic IR spectra ($650\text{--}4000\text{ cm}^{-1}$) under gas flow were measured on Thermo Nicolet 6700 and Thermo Nicolet Continuum spectrometers with a Linkam FTIR600 heating and freezing stage. The samples were directly placed on the BaF_2 plate. XRD data of microcrystals were collected using a Rigaku RINT-Ultima III diffractometer employing $\text{Cu K}\alpha$ radiation. Thermogravimetric analysis (TGA) was performed using a Rigaku ThermoPlus2/TG-DTA8129 over the temperature range from room temperature to $500\text{ }^\circ\text{C}$ under a N_2 flow at a heating rate of 10 K min^{-1} . The adsorption and desorption isotherms for CO_2 (195 K), O_2 , N_2 , and Ar (77 and 195 K) were recorded on a BELSORP-max volumetric adsorption instrument (BEL Japan, Inc.). The adsorption and desorption isotherms for H_2O at 298 K were measured with BELSORP-aqua volumetric adsorption equipment (BEL Japan, Inc.). Prior to adsorption measurements, the sample was heated at 373 K in a vacuum overnight.

RESULTS AND DISCUSSION

Crystal Structure. 1D2acetone isolated using acetone as the solvent crystallizes in the orthorhombic space group $\text{Cmc}2_1$ (No. 36). Figure 1a shows the unit cell of 1D2acetone viewed along the a axis. The one-dimensional $[\text{Cu}(\text{CF}_3\text{SO}_3)(\text{bpp})_2]_n$ frameworks running along the a axis are arrayed with uncoordinated CF_3SO_3^- anions and guest acetone molecules. The Cu^{II} ion has an elongated square-pyramidal environment with four bpp nitrogen atoms in the equatorial plane and one oxygen atom of the CF_3SO_3^- anion at the axial site (Figure 1b). Although the remaining axial site is occupied by the acetone molecule, the $\text{Cu}\cdots\text{O}$ distance of $3.481(3)\text{ \AA}$ indicates no coordinative interaction. The $\text{Cu}\text{--}\text{O}(\text{CF}_3\text{SO}_3^-)$ bond distance [$2.392(3)\text{ \AA}$] is considerably longer than the $\text{Cu}\text{--}\text{N}$ bond distances [$2.022(3)$ and $2.021(3)\text{ \AA}$] because of a Jahn–Teller distortion. Bond-valence calculations are consistent with the divalent oxidation state of copper and the Jahn–Teller distortion (see Table S1 in the Supporting Information, SI).¹⁰ The bpp ligand can have four different conformations, as mentioned above. In 1D2acetone, there are two crystallographically independent bpp molecules that have the same conformation TT and similar torsion angles (see Figure S1 in the SI). The bpp ligands bridge the Cu^{II} centers to form a one-dimensional doubly linked chain structure running along the a axis (Figure 1c). The intrachain $\text{Cu}\cdots\text{Cu}$ distance is ca. 12.3 \AA . The interchain distances in the b and c directions are ca. 8.6 and 9.6 \AA , respectively (see Figure S2 in the SI). Uncoordinated CF_3SO_3^- anions and acetone molecules are incorporated into the space between the chains via weak hydrogen-bonding interactions (Table S2 in the SI).

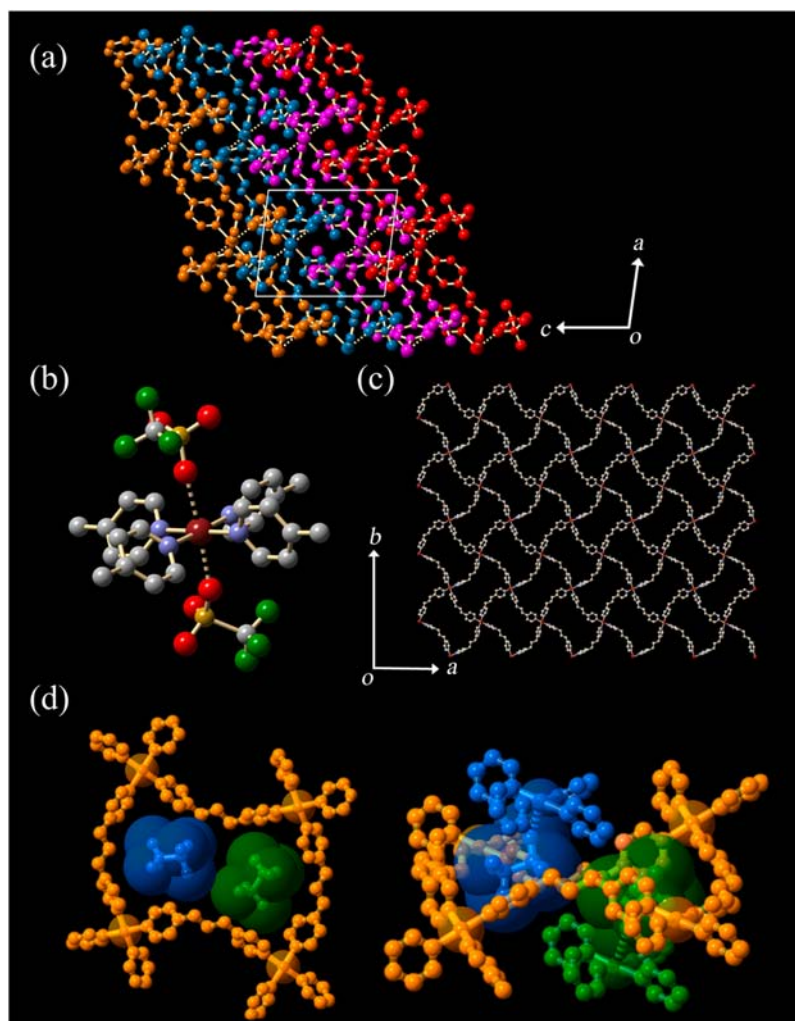


Figure 2. Crystal structure of $2\text{D}\text{H}_2\text{O}$. (a) Unit cell viewed along the b axis. Each two-dimensional layer is depicted in a different color. (b) Coordination environment around the Cu^{II} center. (c) Two-dimensional layer structure projected along the c axis (coordinated CF_3SO_3^- anions are omitted for clarity). (d) View of the inclusion state of the coordinated CF_3SO_3^- anions inside the grid. The CF_3SO_3^- anions of the upper and lower layers are colored in blue and green, respectively. In all figures, the hydrogen atoms are omitted for clarity.

$2\text{D}\text{H}_2\text{O}$ obtained from a $\text{H}_2\text{O}/\text{MeOH}$ solution crystallizes in the monoclinic space group $P2_1$ (No. 4). Figure 2a shows the unit cell of $2\text{D}\text{H}_2\text{O}$ viewed along the b axis, in which the two-dimensional $[\text{Cu}(\text{CF}_3\text{SO}_3)_2(\text{bpp})_2]_n$ layers are stacked incorporating guest H_2O molecules. The structure around the Cu^{II} center is shown in Figure 2b: the Cu^{II} center has an octahedral environment exhibiting a Jahn–Teller axial elongation with four bpp nitrogen atoms in the basal plane [Cu–N distances = 2.029(2), 2.029(2), 2.030(2), and 2.032(2) Å] and two CF_3SO_3^- oxygen atoms at the axial sites [Cu–O distances = 2.427(2) and 2.527(2) Å]. Bond-valence calculations are consistent with the divalent oxidation state of copper and the Jahn–Teller distortion (see Table S3 in the SI).¹⁰ In $2\text{D}\text{H}_2\text{O}$, there are two crystallographically independent bpp molecules. Although both have the same conformation TT, their torsion angles are slightly different (see Figure S3 in the SI). The bpp ligands bridge the Cu^{II} centers to form two-dimensional layers with distorted rectangular grids, as illustrated in Figure 2c. The intrasheet Cu⋯Cu distances are ca. 13.4 and 15.7 Å. Each two-dimensional layer stacks, in which one grid is filled by two CF_3SO_3^- anions of the upper and lower layers and one guest H_2O molecule (Figure 2d). The guest H_2O molecule is located in an isolated cavity and interacts with coordinated CF_3SO_3^-

anions via hydrogen bonds [O⋯O = 2.682(7) and 2.895(6) Å], as shown in Figures S4 and S5 in the SI. The accessible void space calculated by the PLATON program is 3.3%.¹¹ The calculated pore volume is $0.023 \text{ cm}^3 \text{ g}^{-1}$.

The reaction in a DMF/toluene solution afforded $3\text{D}\text{DMF}\cdot\text{toluene}$ crystallized in the monoclinic space group $P2_1/n$ (No. 14). Figure 3a shows the unit cell of $3\text{D}\text{DMF}\cdot\text{toluene}$ viewed along the b axis, where the one-dimensional $[\text{Cu}(\text{CF}_3\text{SO}_3)(\text{bpp})_2(\text{DMF})]_n$ frameworks running along the b axis are arranged with uncoordinated CF_3SO_3^- anions and guest toluene molecules. The Cu^{II} center is coordinated to four pyridine nitrogen atoms from the bpp ligands [Cu–N distances = 2.019(4), 2.024(4), 2.029(4), and 2.044(4) Å] on the equatorial plane and two oxygen atoms from one CF_3SO_3^- anion [Cu–O distance = 2.669(4) Å] and one DMF molecule [Cu–O distance = 2.431(4) Å] at the axial sites with a Jahn–Teller elongation (Figure 3b). Bond-valence calculations are consistent with the divalent oxidation state of copper and the Jahn–Teller distortion (see Table S5 in the SI).¹⁰ In contrast to $1\text{D}\text{acetone}$ and $2\text{D}\text{H}_2\text{O}$, there are two kinds of bpp conformations, TT and TG, in $3\text{D}\text{DMF}\cdot\text{toluene}$ (Figure S6 in the SI). The Cu^{II} centers are linked by bpp ligands, forming a one-dimensional doubly linked chain

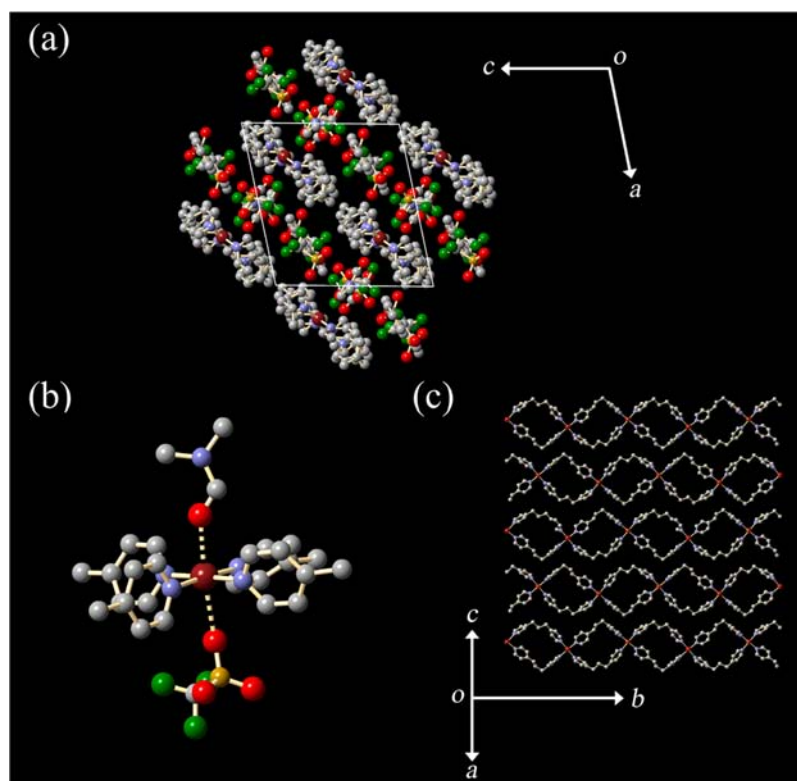


Figure 3. Crystal structure of 3D2DMF-toluene. (a) Unit cell viewed along the b axis. (b) Coordination environment around the Cu^{II} center. (c) One-dimensional doubly linked chain structure projected along the $a + c$ direction (DMF and CF_3SO_3^- molecules are omitted for clarity). In all figures, the hydrogen atoms are omitted for clarity.

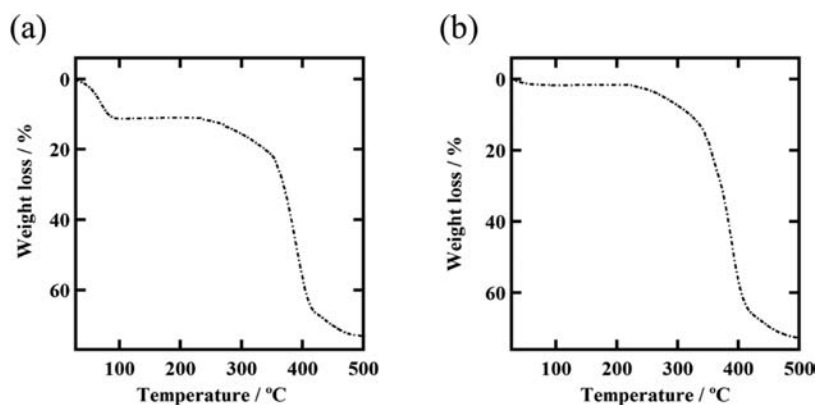


Figure 4. TGA curves of (a) 1D2acetone and (b) 2D2H₂O.

structure that has a grid shape slightly different from that of 1D2acetone (Figure 3c). The intrachain $\text{Cu}\cdots\text{Cu}$ distance is ca. 11.7 Å. The interchain distances in the $a-c$ and $a + c$ directions are ca. 10.6 and 8.5 Å, respectively (see Figure S7 in the SI). There are uncoordinated CF_3SO_3^- anions and toluene molecules in the space between the chains via weak hydrogen-bonding interactions (Table S6 in the SI).

TGA and XRD. The result of TGA in 1D2acetone suggests that all acetone molecules are released in the temperature range from room temperature to 100 °C (obsd 11.3%) and that the resultant desolvated solid **1** is stable up to ~220 °C, without further weight loss, as shown in Figure 4a. The slight difference in the observed and calculated acetone contents (13.3% for 1D2acetone) is caused by the partial removal of acetone molecules from the as-synthesized 1D2acetone in air. The powder XRD pattern of the desolvated solid **1**, which was

obtained by heating 1D2acetone at 100 °C in a vacuum, shows sharp lines with shifting of some Bragg peak positions in comparison with the as-synthesized 1D2acetone and the simulated 1D2acetone from single-crystal analysis (Figure 5), indicating no destruction but structural change of the framework upon desolvation. However, when the desolvated **1** is exposed to acetone vapor, it reverts to the original 1D2acetone, which was detected by XRD (Figure 5c). Hence, it is concluded that **1** possesses a flexible framework, reversibly responding to an acetone guest molecule.

The TGA curve of 2D2H₂O shows a weight loss of 1.6% from room temperature to 100 °C (Figure 4b). This corresponds to a loss of 0.7 H₂O molecule per formula unit. The slight difference in the observed and calculated H₂O contents (2.3% for 2D2H₂O) is caused by the partial removal of H₂O molecules from the as-synthesized 2D2H₂O in air. To check the adsorption

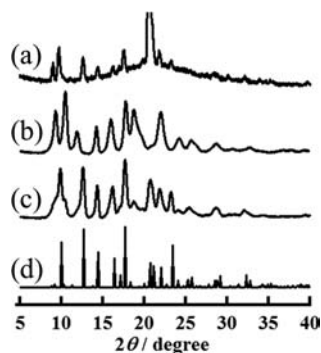


Figure 5. XRD patterns of (a) as-synthesized 1D2acetone, (b) **1**, and (c) 1D2acetone obtained by exposure of **1** to saturated acetone vapor and (d) simulated pattern of 1D2acetone.

behavior of H₂O, the adsorption and desorption isotherms for H₂O at 298 K in **2** were measured (Figure S9 in the SI). The isotherms indicate that the H₂O content is dependent on humidity. After the removal of H₂O molecules, no obvious weight loss steps occurred below 220 °C, indicating that the desolvated structure of **2** is stable up to this temperature. The decomposition temperatures of **1** and **2** are similar to each other despite their different framework dimensionalities. The powder XRD pattern of the desolvated **2**, which was obtained by drying as-synthesized 2D₂H₂O in a vacuum at 100 °C, shows sharp peaks at positions similar to those of the as-synthesized 2D₂H₂O and the simulated 2D₂H₂O from single-crystal analysis (Figure 6), indicating that the desolvated **2** maintains its framework after the removal of H₂O molecules.

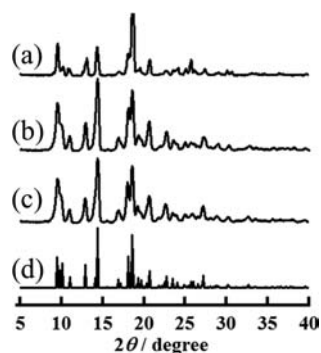


Figure 6. XRD patterns of (a) as-synthesized 2D₂H₂O, (b) **2**, and (c) 2D₂H₂O obtained by exposure of **2** to saturated H₂O vapor and (d) simulated pattern of 2D₂H₂O.

It is worth noting that guest H₂O molecules are easily removed from the isolated cavities in 2D₂H₂O. The release of guest H₂O molecules from the isolated cavities requires an expansion of the framework, which would be clearly manifested in a change of the lattice parameters, but the powder XRD data (Figure 6) showed no change in the crystal structure in response to the ingress and loss of H₂O. The translation of H₂O from isolated cavities must therefore proceed by expansion of the framework for only as long as is required for translation of the guest H₂O molecule. The structure then relaxes to its original form. It is important to recall that the porous framework is thermally stable to 220 °C, demonstrating that the guest molecules are dynamically distorting an intrinsically stable structure. The reason for such dynamics is probably that the cavities are created by assembling the two-

dimensional layers via weak C–H···O hydrogen bonds between the oxygen atoms of the CF₃SO₃[−] anions and the bpp ligands at a distance of 3.288(5)–3.480(4) Å. Similar unique framework dynamics have been reported for other PCPs, [Ni₂(4,4'-bpy)₃(NO₃)₄]_n¹² and [Ni₂(NCX)₄(azpy)₄]_n [X = S and Se; azpy = 4,4'-azobis(pyridine)].¹³ One-dimensional ladder structures of [Ni₂(4,4'-bpy)₃(NO₃)₄]_n are assembled by C–H···O hydrogen bonds between the oxygen atoms of the NO₃[−] anions and the 4,4'-bpy ligands at a distance of 2.72(2) Å, while [Ni₂(NCX)₄(azpy)₄]_n is an aggregate of two-dimensional frameworks via an interpenetration that is not a chemically bonded network but is merely a mechanical entanglement. Such characteristic dynamics in **2** cause the different adsorption behavior from **1** (vide infra).

IR. ATR-IR spectra were measured to clarify the coordination state of the CF₃SO₃[−] anions. Figure 7 represents

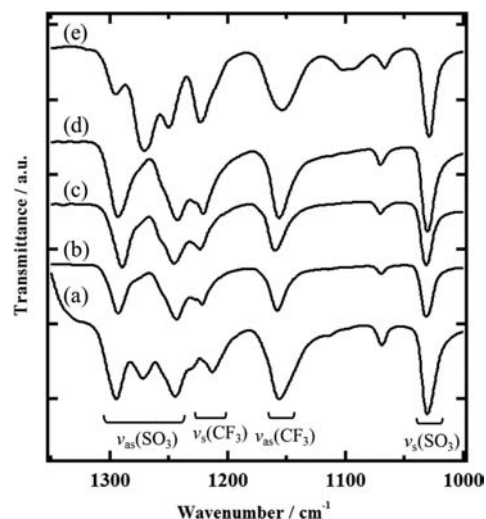


Figure 7. ATR-IR spectra of (a) 1D2acetone, (b) **1**, (c) 2D₂H₂O, (d) **2**, and (e) 3DDMF-toluene.

the ATR-IR spectra of 1D2acetone, 2D₂H₂O, desolvated **1** and **2**, and 3DDMF-toluene. The characteristic bands for the asymmetric $\nu_{as}(\text{SO}_3)$ stretching modes of CF₃SO₃[−] anions appeared at 1295, 1272, and 1244 cm^{−1} for 1D2acetone, 1290 and 1246 cm^{−1} for 2D₂H₂O, 1293 and 1243 cm^{−1} for **1**, 1293 and 1243 cm^{−1} for **2**, and 1295, 1271, and 1250 cm^{−1} for 3DDMF-toluene, while the symmetric $\nu_s(\text{SO}_3)$ stretching bands were observed at 1031 cm^{−1} (1D2acetone), 1032 cm^{−1} (2D₂H₂O), 1032 cm^{−1} (**1**), 1030 cm^{−1} (**2**), and 1029 cm^{−1} for 3DDMF-toluene.¹⁴ It has been reported that the symmetry of the CF₃SO₃[−] anion is lowered when coordinated to metal ions, such as Pb^{II}, Zn^{II}, and Ni^{II}, causing a splitting of the asymmetric $\nu_{as}(\text{SO}_3)$ stretching band into two components {1298 and 1234 cm^{−1} ($\Delta\nu = 64$ cm^{−1}) for Pb(CF₃SO₃)₂-PEO [PEO = poly(ethylene oxide)], 1322 and 1238 cm^{−1} ($\Delta\nu = 84$ cm^{−1}) for Zn(CF₃SO₃)₂-PEO, and 1320 and 1236 cm^{−1} ($\Delta\nu = 84$ cm^{−1}) for Ni(CF₃SO₃)₂-PEO}.¹⁵ The desolvated **1** shows splitting ($\Delta\nu = 50$ cm^{−1}) similar to those of 2D₂H₂O ($\Delta\nu = 44$ cm^{−1}) and **2** ($\Delta\nu = 50$ cm^{−1}). 1D2acetone and 3DDMF-toluene have both coordinated and uncoordinated CF₃SO₃[−] anions, and their asymmetric $\nu_{as}(\text{SO}_3)$ stretching modes are observed at 1295 and 1244 cm^{−1} ($\Delta\nu = 51$ cm^{−1}, coordinated CF₃SO₃[−]) and 1272 cm^{−1} (uncoordinated CF₃SO₃[−]) for 1D2acetone and at 1295 and 1250 cm^{−1} ($\Delta\nu = 45$ cm^{−1}, coordinated CF₃SO₃[−]) and 1271 cm^{−1} (uncoordinated

CF_3SO_3^-) for $3\text{DDMF}\cdot\text{toluene}$. Hence, these results indicate that in **1** the originally uncoordinated CF_3SO_3^- anion approaches and weakly coordinates to the axial site formed after removal of the acetone guest and that the resulting desolvated **1** has an elongated octahedral environment similar to those of $2\text{D}_2\text{O}$ and **2**, that is, only coordinated CF_3SO_3^- anions, as shown in Figure 8. The splitting for $1\text{D}_2\text{acetone}$,

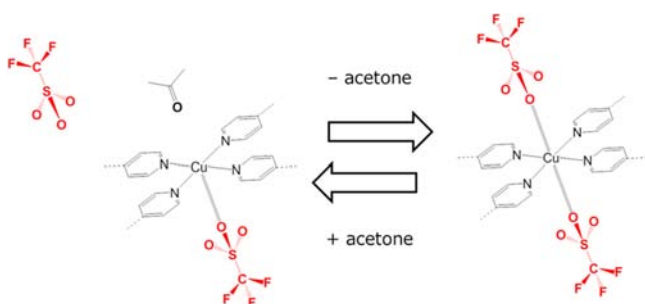


Figure 8. Structural change around the Cu^{II} center before and after the removal of acetone guest molecules in $1\text{D}_2\text{acetone}$.

$2\text{D}_2\text{O}$, **1**, **2**, and $3\text{DDMF}\cdot\text{toluene}$ is smaller than that for $\text{M}(\text{CF}_3\text{SO}_3)_2\text{-PEO}$ ($\text{M} = \text{Pb}^{\text{II}}$, Zn^{II} , and Ni^{II}) systems because their axial $\text{Cu}\cdots\text{CF}_3\text{SO}_3$ interactions are weaker.

Adsorption Properties. We measured the adsorption and desorption isotherms for CO_2 , O_2 , Ar, and N_2 . The adsorption isotherm for CO_2 at 195 K in **1** showed a sudden increase at the gate-opening pressure $P_{\text{go}} = 60$ kPa and attained saturation of $153 \text{ cm}^3(\text{STP}) \text{ g}^{-1}$ (5.2 mol mol^{-1}), as shown in Figure 9a. The Langmuir surface area is $1004 \text{ m}^2 \text{ g}^{-1}$, which is comparable with the highest value for zeolites ($904 \text{ m}^2 \text{ g}^{-1}$)¹⁶ and higher than those for all other one-dimensional PCPs.¹⁷ The desorption isotherm of CO_2 showed the adsorption volume decreasing at lower pressure and a large hysteresis loop. These results reveal that **1** has a close-packing structure that prohibits the diffusion of CO_2 gas molecules inside the framework at pressures below P_{go} and the structure is transformed from a closed form to an open form that can take CO_2 gas molecules at P_{go} , as illustrated in Figure 10. On the other hand, **1** showed almost no O_2 , Ar, and N_2 adsorption at 195 K over a pressure range up to 100 kPa. At 77 K, O_2 gas was adsorbed on **1** with the gate-opening adsorption process ($P_{\text{go}} = 0.9$ kPa), as shown in Figure 9b, while N_2 and Ar gases were not adsorbed. Such a guest dependency of P_{go} is consistent with the order of the boiling points (194.7, 90.2, 87.3, and 77.4 K for CO_2 , O_2 , Ar, and N_2 , respectively), which suggests that the intermolecular interaction force of the guest molecules governs this gate-opening process. Similar adsorption behaviors have been observed in flexible two- and three-dimensional PCPs.¹⁸

2 showed a rapid increase in the adsorbed amount of CO_2 gas at 195 K and low pressure (Figure 11). The saturated adsorbed amount of CO_2 is $28 \text{ cm}^3(\text{STP}) \text{ g}^{-1}$, which corresponds to roughly one CO_2 molecule per formula unit ($0.95 \text{ mol mol}^{-1}$). Note that CO_2 is smoothly adsorbed to isolated cavities of **2**, which requires an expansion of the framework, that is, a gate-opening process. If the intermolecular interaction force of the guest molecules governs this gate-opening process, O_2 gas could be adsorbed, as is the case in **1**. However, O_2 , Ar, and N_2 gases were not adsorbed to **2** at 195 or 77 K (Figures 11 and S10 in the SI). Although the structure of CO_2 -adsorbed **2** is unknown, we here propose an adsorption mechanism in **2**. The saturated adsorbed amount of CO_2 ($0.95 \text{ mol per formula unit}$) is comparable with the amount of H_2O guests incorporated in $2\text{D}_2\text{O}$ ($1 \text{ mol per formula unit}$), which suggests that one cavity in **2** incorporates just one CO_2 molecule in a commensurate fashion. Because the calculated molecular volume of CO_2 (45.0 \AA^3) is larger than that of H_2O (27.7 \AA^3),¹⁹ CO_2 -adsorbed **2** will have a slightly larger unit cell than $2\text{D}_2\text{O}$. In contrast, O_2 , Ar, and N_2 with smaller molecular volumes (30.6 , 33.5 , and 36.6 \AA^3 , respectively)¹⁹ were not adsorbed, which indicates that the molecular volume of gases is not the main factor in determining adsorption selectivity in **2**. This may therefore be attributed to the difference in the molecular sizes of gases (Lennard-Jones parameters: CO_2 , 2.98 \AA ; O_2 , 3.11 \AA ; Ar, 3.40 \AA ; N_2 , 3.32 \AA).²⁰ Each two-dimensional layer stacks tightly by filling two CF_3SO_3^- anions of the upper and lower layers into one grid, which gives a limit for temporary expansion of the framework. Thereby, **2** permits only the small CO_2 molecule to diffuse within the frameworks with temporary expansion, as illustrated in Figure 12.

Here, we discuss adsorption sites for gas molecules. As mentioned in the IR section, the desolvated **1** and **2** have similar $(4 + 2) [\text{CuN}_4\text{O}_2]$ coordination environments (Figure 8). One possible adsorption site is an inorganic fluorinated CF_3SO_3^- anion. The inorganic fluorinated CF_3SO_3^- anion employed in this study has been used as a counteranion of ionic liquids.^{21,22} It is known that a CO_2 molecule interacts with this anion via an acid–base interaction in ionic liquids.²¹ Another possible adsorption site is an open Cu^{II} site. There have been some examples that report interactions between open metal sites and CO_2 molecules.²³ The desolvated **1** and **2** have no open Cu^{II} sites, as mentioned above. If weakly coordinated CF_3SO_3^- anions are displaced with CO_2 molecules, $\text{Cu}^{\text{II}}\cdots\text{CO}_2$ interactions would be formed. To clarify such a displacement, we measured IR spectra of CO_2 -adsorbed **1** and **2** (see Figure S11 in the SI). The characteristic IR bands derived from uncoordinated CF_3SO_3^- anions were not observed for both CO_2 -adsorbed samples, supporting that the adsorption of CO_2 scarcely has an effect on the coordination environments of

Table 2. Characteristic IR Bands in $1\text{D}_2\text{acetone}$, **1**, $2\text{D}_2\text{O}$, **2**, and $3\text{DDMF}\cdot\text{toluene}$

assignments	IR frequencies (cm^{-1})				
	$1\text{D}_2\text{acetone}$	1	$2\text{D}_2\text{O}$	2	$3\text{DDMF}\cdot\text{toluene}$
$\nu_{\text{as}}(\text{SO}_3)$ band (coordinated CF_3SO_3^-)	1295	1293	1290	1293	1295
	1244	1243	1246	1243	1250
$\nu_{\text{as}}(\text{SO}_3)$ band (uncoordinated CF_3SO_3^-)	1272				1271
$\nu_{\text{s}}(\text{SO}_3)$ band	1031	1032	1032	1030	1029
$\nu_{\text{as}}(\text{CF}_3)$ band	1157	1158	1160	1157	1154
$\nu_{\text{s}}(\text{CF}_3)$ band	1220	1222	1224	1221	1223

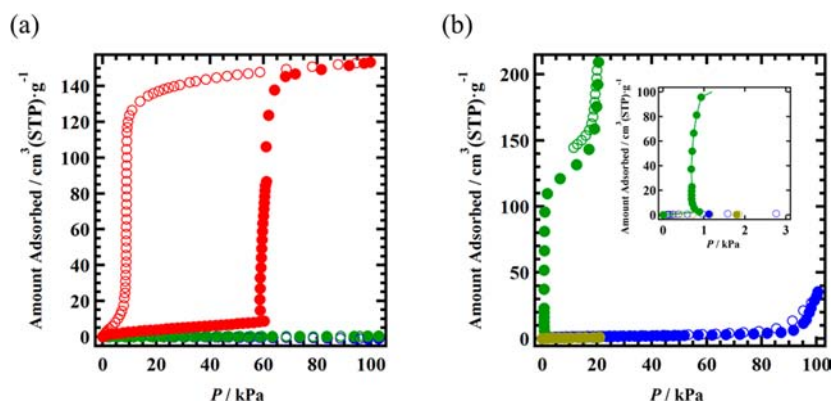


Figure 9. (a) Adsorption and desorption isotherms for CO₂ (red), O₂ (green), Ar (gold), and N₂ (blue) of 1 at 195 K. The isotherms for O₂, Ar, and N₂ overlap. (b) Adsorption and desorption isotherms for O₂ (green), Ar (gold), and N₂ (blue) of 1 at 77 K. Adsorption and desorption points are represented by filled and open symbols, respectively.

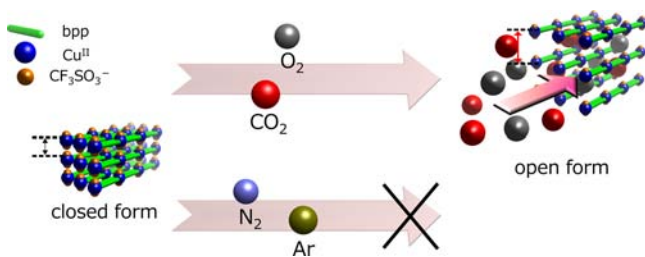


Figure 10. Proposed adsorption mechanism in 1.

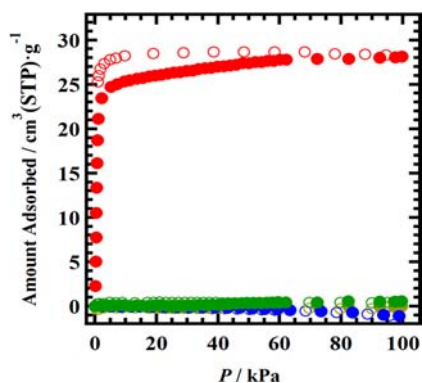


Figure 11. Adsorption (filled symbols) and desorption (open symbols) isotherms for CO₂ (red), O₂ (green), Ar (gold), and N₂ (blue) of 2 at 195 K. The isotherms for O₂ and Ar overlap.

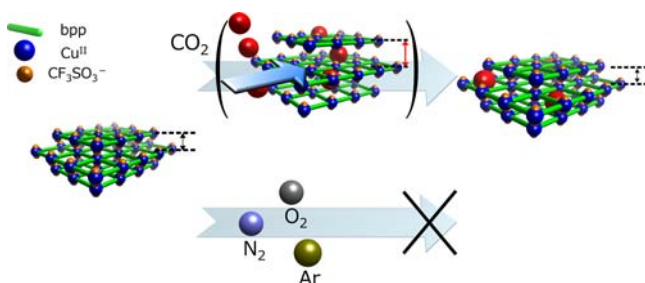


Figure 12. Proposed adsorption mechanism in 2.

CF₃SO₃⁻ anions. Similar behaviors have been observed in related PCPs, [Cu(PF₆)₂(1,2-bis(4-pyridyl)ethane)₂]_n and [Cu(BF₄)₂(4,4'-bpy)₂]_n.^{17b,24} Hence, the adsorption sites in 1 and 2 are probably inorganic fluorinated CF₃SO₃⁻ anions.

CONCLUSION

Control of the polymorphs has so far been a significant challenge in bringing out diverse structures and functions from a particular compound.^{2–5,25} In this work, we synthesized novel PCP polymorphs, [Cu(CF₃SO₃)₂(bpp)₂]_n, by using a flexible and bent bpp ligand. Different solvent systems afforded the precursors of polymorphs, 1D acetone and 2D H₂O. 1D acetone possessed a one-dimensional doubly linked chain structure, while 2D H₂O formed two-dimensional layers. The two polymorphs 1 and 2 obtained after the removal of guest molecules by heating the precursors in a vacuum showed not only different assembled structures but also different gate-opening adsorption properties. The adsorption to 1 is accompanied with a structural transformation from closed to open forms, while 2 adsorbed guests with an expansion of the framework for only as long as is required for the passage of guest molecules. To the best of our knowledge, this PCP polymorph showing either of two different types of flexible pores is a very rare example. This synthetic approach could contribute to further diversification of the PCP properties.

ASSOCIATED CONTENT

Supporting Information

Structural figures, TGA curve of 3DMF·toluene, adsorption and desorption isotherms for H₂O (298 K) and O₂, Ar, and N₂ (77 K) of 2, IR spectra of CO₂-adsorbed 1 and 2, bond-valence parameters, hydrogen-bonding distances, and X-ray crystallographic data in CIF format. This material is available free of charge via the Internet at <http://pubs.acs.org>.

AUTHOR INFORMATION

Corresponding Author

*E-mail: noro@es.hokudai.ac.jp (S.N.), tnaka@es.hokudai.ac.jp (T.N.).

Notes

The authors declare no competing financial interest.

ACKNOWLEDGMENTS

The authors gratefully thank Prof. M. Kato, Prof. H.-C. Chang, and Dr. A. Kobayashi (Hokkaido University, Sapporo, Japan) for collecting temperature-dependent microscopic IR data. The authors thank Tomo Hattori (Instrumental Analysis Division, Equipment Management Center, Creative Research Institution, Hokkaido University) for carrying out elemental analysis. This

work is supported by PRESTO-JST and a Grant-in-Aid for Scientific Research from MEXT, Japan.

REFERENCES

- (1) (a) Kitagawa, S.; Kitaura, R.; Noro, S. *Angew. Chem., Int. Ed.* **2004**, *43*, 2334–2375. (b) Noro, S.; Kitagawa, S.; Akutagawa, T.; Nakamura, T. *Prog. Polym. Sci.* **2009**, *34*, 240–279. (c) Férey, G. *ChemSusChem* **2008**, *37*, 191–214. (d) Horike, S.; Shimomura, S.; Kitagawa, S. *Nat. Chem.* **2009**, *1*, 695–704. (e) Kanoo, P.; Ghosh, A. C.; Cyriac, S. T.; Maji, T. K. *Chem.—Eur. J.* **2012**, *18*, 237–244. (f) Seeber, G.; Cooper, G. J. T.; Newton, G. N.; Rosnes, M. H.; Long, D.-L.; Kariuki, B. M.; Kögerler, P.; Cronin, L. *Chem. Sci.* **2010**, *1*, 62–67. (g) Zacher, D.; Schmid, R.; Wöll, C.; Fischer, R. A. *Angew. Chem., Int. Ed.* **2011**, *50*, 176–199. (h) Lu, G.; Li, S.; Guo, Z.; Hauser, B. G.; Farha, O. K.; Qi, X.; Wang, Y.; Wang, X.; Liu, X.; Zhang, H.; Zhang, Q.; Chen, X.; Ma, J.; Joachim, L.; Yang, Y.; Hupp, J. T.; Huo, F. *Nat. Chem.* **2012**, *4*, 310–316. (i) Motokawa, N.; Matsunaga, S.; Takaishi, S.; Miyasaka, H.; Yamashita, M.; Dunbar, K. R. *J. Am. Chem. Soc.* **2010**, *132*, 11943–11951.
- (2) (a) Dybtsev, D. N.; Chun, H.; Kim, K. *Angew. Chem., Int. Ed.* **2004**, *43*, 5033–5036. (b) Chun, H.; Moon, J. *Inorg. Chem.* **2007**, *46*, 4371–4373. (c) Friščić, T.; Reid, D. G.; Halasz, I.; Stein, R. S.; Dinnebier, R. E.; Duer, M. J. *Angew. Chem., Int. Ed.* **2010**, *49*, 712–715. (d) Kondo, M.; Takashima, Y.; Seo, J.; Kitagawa, S.; Furukawa, S. *CrystEngComm* **2012**, *12*, 2350–2353.
- (3) Bureekaew, S.; Sato, H.; Matsuda, R.; Kubota, Y.; Hirose, R.; Kim, J.; Kato, K.; Takata, M.; Kitagawa, S. *Angew. Chem., Int. Ed.* **2010**, *49*, 7660–7664.
- (4) Wang, X.-S.; Ma, S.; Forster, P. M.; Yuan, D.; Eckert, J.; López, J. J.; Murphy, B. J.; Parise, J. B.; Zhou, H.-C. *Angew. Chem., Int. Ed.* **2008**, *47*, 7263–7266.
- (5) (a) Kondo, A.; Kajiro, H.; Noguchi, H.; Carlucci, L.; Proserpio, D. M.; Ciani, G.; Kato, K.; Takata, M.; Seki, H.; Sakamoto, M.; Hattori, Y.; Okino, F.; Maeda, K.; Ohba, T.; Kaneko, K.; Kanoh, H. *J. Am. Chem. Soc.* **2011**, *133*, 10512–10522. (b) Gándara, F.; de la Peña-O’Shea, V. A.; Illas, F.; Snejko, N.; Proserpio, D. M.; Gutiérrez-Puebla, E.; Monge, M. A. *Inorg. Chem.* **2009**, *48*, 4707–4713. (c) Caskey, S. R.; Wong-Foy, A. G.; Matzger, A. J. *Inorg. Chem.* **2008**, *47*, 7751–7756.
- (6) (a) Carlucci, L.; Ciani, G.; Proserpio, D. M.; Rizzato, S. *CrystEngComm* **2002**, *4*, 121–129. (b) Hu, L.; Slebođnick, C.; Gandour, R. D.; Hanson, B. E. *Inorg. Chim. Acta* **2008**, *361*, 2439–2446. (c) Erdođdu, Y.; Tahir, G. M.; Kurt, M. *Spectrochim. Acta A* **2008**, *71*, 377–387. (d) Hu, L.; Slebođnick, C.; Gandour, R. D.; Hanson, B. E. *Inorg. Chim. Acta* **2008**, *361*, 2439–2446.
- (7) (a) Carlucci, L.; Ciani, G.; Moret, M.; Proserpio, D. M.; Rizzato, S. *Chem. Mater.* **2002**, *14*, 12–16. (b) Lue, G.-G.; Xiong, H.-B.; Dai, J.-C. *Cryst. Growth Des.* **2011**, *11*, 507–515. (c) Luo, F.; Che, Y.-X.; Zheng, J.-m. *J. Mol. Struct.* **2007**, *828*, 162–165. (d) Ryu, J. Y.; Kim, C.; Park, D. W.; Park, L. O.; Kim, Y.; Lough, A. J. *Acta Crystallogr., Sect. E* **2005**, *61*, m1489–m1491.
- (8) (a) Wiberg, K. B.; Keith, T. A.; Frisch, M. J.; Murcko, M. J. *Phys. Chem.* **1995**, *99*, 9072–9079. (b) Kent, D. R., IV; Dey, N.; Davidson, F.; Gregoire, F.; Petterson, K. A.; Goddard, W. A., III; Roberts, J. D. J. *Am. Chem. Soc.* **2002**, *124*, 9318–9322. (c) Lee, J. Y.; Yoshida, N.; Hirata, F. *J. Phys. Chem. B* **2006**, *110*, 16018–16025.
- (9) Sheldrick, G. M. *SHELXS-97 and SHELXL-97: Program for the Solution and Refinement of Crystal Structures*; University of Göttingen: Göttingen, Germany, 1997.
- (10) Brown, I. D.; Altermatt, D. *Acta Crystallogr., Sect. B* **1985**, *41*, 244–247.
- (11) The accessible void space was calculated after the removal of all guest molecules with the program PLATON by using a probe with a radius of 1.2 Å. Spek, A. L. *J. Appl. Crystallogr.* **2003**, *36*, 7–13.
- (12) (a) Kepert, C. J.; Rosseinsky, M. J. *Chem. Commun.* **1999**, 375–376. (b) Fletcher, A. J.; Cussen, E. J.; Prior, T. J.; Rosseinsky, M. J.; Kepert, C. J.; Thomas, K. M. *J. Am. Chem. Soc.* **2001**, *123*, 10001–10011.
- (13) Noro, S.; Kitaura, R.; Kitagawa, S.; Akutagawa, T.; Nakamura, T. *Inorg. Chem.* **2006**, *45*, 8990–8997.
- (14) Huang, W.; Frech, R.; Wheeler, R. A. *J. Phys. Chem.* **1994**, *98*, 100–110.
- (15) Wendsjö, Å.; Thomas, J. O.; Lindgren, J. *Polymer* **1993**, *34*, 2243–2249.
- (16) Chester, A. W.; Clement, P.; Han, S. U.S. Patent Appl. 2000/6136291A, 2006.
- (17) (a) Takamizawa, S.; Hiroki, T.; Nakata, E.; Mochizuki, K.; Mori, W. *Chem. Lett.* **2002**, 1208–1209. (b) Noro, S.; Tanaka, D.; Sakamoto, H.; Shimomura, S.; Kitagawa, S.; Takeda, S.; Uemura, K.; Kita, H.; Akutagawa, T.; Nakamura, T. *Chem. Mater.* **2009**, *21*, 3346–3355.
- (18) (a) Kitaura, R.; Seki, K.; Akiyama, G.; Kitagawa, S. *Angew. Chem., Int. Ed.* **2003**, *42*, 428–431. (b) Tanaka, D.; Nakagawa, K.; Higuchi, M.; Horike, S.; Kubota, Y.; Kobayashi, T. C.; Takata, M.; Kitagawa, S. *Angew. Chem., Int. Ed.* **2008**, *47*, 3914–3918. (c) Llewellyn, P. L.; Horcajada, P.; Maurin, G.; Devic, T.; Rosenbach, N.; Bourrelly, S.; Serre, C.; Vincent, D.; Loera-Serna, S.; Filinchuk, Y.; Frey, G. *J. Am. Chem. Soc.* **2009**, *131*, 13002–13008.
- (19) Kitaura, R.; Matsuda, R.; Kubota, Y.; Kitagawa, S.; Takata, M.; Kobayashi, T. C.; Suzuki, M. *J. Phys. Chem. B* **2005**, *109*, 23378–23385.
- (20) Vrabec, J.; Stoll, J.; Hasse, H. *J. Phys. Chem. B* **2001**, *105*, 12126–12133.
- (21) Bhargava, B. L.; Balasubramanian, S. *Chem. Phys. Lett.* **2007**, *444*, 242–246.
- (22) (a) Cammarata, L.; Kazarian, S. G.; Salter, P. A.; Welton, T. *Phys. Chem. Chem. Phys.* **2001**, *3*, 5192–5200. (b) Aki, S. N. V. K.; Mellein, B. R.; Saurer, E. M.; Brennecke, J. F. *J. Phys. Chem. B* **2004**, *108*, 20355–20365. (c) Kazarian, S. G.; Briscoe, B. J.; Welton, T. *Chem. Commun.* **2000**, 2047–2048.
- (23) (a) Bordiga, S.; Regli, L.; Bonino, F.; Groppo, E.; Lamberti, C.; Xiao, B.; Wheatley, P. S.; Morris, R. E.; Zecchina, A. *Phys. Chem. Chem. Phys.* **2007**, *9*, 2676–2685. (b) Llewellyn, P. L.; Bourrelly, S.; Serre, C.; Vimont, A.; Daturi, M.; Hamon, L.; Weireld, G. D.; Chang, J.-S.; Hong, D. Y.; Hwang, Y. K.; Jhung, S. H.; Férey, G. *Langmuir* **2008**, *24*, 7245–7250. (c) Dietzel, P. D. C.; Johnsen, R. E.; Fjellvag, H.; Bordiga, S.; Groppo, E.; Chavan, S.; Blom, R. *Chem. Commun.* **2008**, 5125–5127.
- (24) Kondo, A.; Noguchi, H.; Ohnishi, S.; Kajiro, H.; Tohdoh, A.; Hattori, Y.; Xu, W.-C.; Tanaka, H.; Kanoh, H.; Kaneko, K. *Nano Lett.* **2006**, *6*, 2581–2584.
- (25) Avendano, C.; Zhang, Z.; Ota, A.; Zhao, H.; Dunbar, K. R. *Angew. Chem., Int. Ed.* **2011**, *50*, 6543–6547.